

# Control of Structural, Electronic, and Optical Properties of Eumelanin Films by Electrospray Deposition

M. Abbas,<sup>†</sup> M. Ali,<sup>‡</sup> S. K. Shah,<sup>‡</sup> F. D'Amico,<sup>§</sup> P. Postorino,<sup>||</sup> S. Mangialardo,<sup>||</sup> M. Cestelli Guidi,<sup>⊥</sup> A. Cricenti,<sup>#</sup> and R. Gunnella<sup>\*,‡,#</sup>

<sup>†</sup>Linz Institute for Organic Solar Cells (LIOS), Johannes Kepler University Linz, Alltenberger Strasse 69, A-4040 Linz, Austria

<sup>‡</sup>School of Science and Technology and CNISM, University of Camerino, Via Madonna delle Carceri 62032 Camerino (MC), Italy

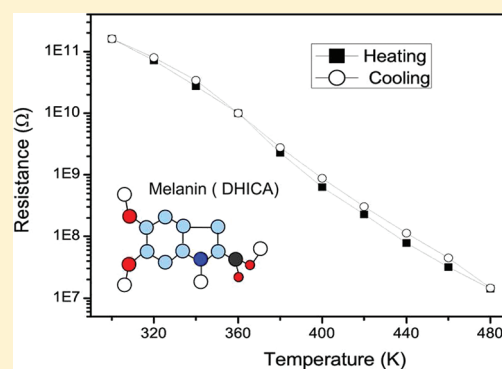
<sup>§</sup>Sincrotrone Trieste S.CpA Strada Statale 14 - Km 163.5 in Area Science Park 34012 Basovizza, Trieste, Italy

<sup>||</sup>Department of Physics, University of Rome -La Sapienza, P.le Aldo Moro, Italy

<sup>⊥</sup>LNF-INFN Via Enrico Fermi, 40 00044 Frascati (RM), Italy

<sup>#</sup>CNR-ISM, Via del Fosso del Cavaliere, 100 - 00133 Roma, Italy

**ABSTRACT:** The capability to monitor finely the physical properties of eumelanin, an important class of biopolymers, involved in melanoma cancer pathologies, whose function and intrinsic disorder still collects the interest of many investigators, was achieved by means of electrospray deposition (ESD). By alleviating the problem of the solubility of melanin through the realization of high-quality films it was possible to spread light on the unknown biopolymer supramolecular organization. In fact, on the basis of scanning probe microscopies, electron spectroscopies, and transport properties, it was possible to delineate peculiar features of the melanin organization varying from heteropolymeric to oligomeric in character and eventually turning in a cross-linked secondary molecular structure.



## I. INTRODUCTION

Eumelanin represents a class of pigments<sup>1,2</sup> that has been collecting many attentions for 50 years after the first studies on purified natural samples.<sup>3,4</sup> From the biochemical point of view, the function of melanin as well as the ambiguous role as a photo-protective agent and the frequency in malignant skin lesions with respect to other melanins like pheomelanin are still unclear.

Very recently, interest in melanin implementations for biodevices as organic sensors, bioelectronics components,<sup>5,6</sup> smart coatings,<sup>7</sup> and biomaterials<sup>8</sup> was renewed by the achievement of device quality films deposition.<sup>9</sup>

For these latter studies, because of the intrinsic heterogeneity, natural melanin was necessarily replaced by synthetic melanin, hopefully able to mimic as close as possible the biological functions.<sup>10</sup>

In this form, eumelanin showed relatively high electrical conductivity,<sup>11</sup> with remarkable threshold switching behavior.<sup>6,12</sup> Strong broadband optical absorption and photoconductivity (PC)<sup>13,14</sup> are related to its ability to convert energy into heat, precluding to applications in highly sensitive bolometers.<sup>15</sup>

We expect that a more detailed investigation of fundamental issues related to this material, like the secondary structure and the functional behavior, will now be available as a reasonable quality of the film is accessible. Further advancement steps in device fabrication necessarily will pass through advances in

isolation, purification and synthesis methods, molecular imaging, and characterization techniques.<sup>16,17</sup>

For instance, Bothma et al. obtained device-quality synthetic eumelanin films<sup>9</sup> by optimizing the use of solvents, and Borghetti et al. obtained device-quality synthetic eumelanin films by the combination of growth techniques and specific assisting elements able to improve the morphological property of the resulting films.<sup>18</sup>

The route to the synthesis of melanin starts from tyrosine and the tyrosinase enzyme. The processes involved are hydroxylation, oxidation, and carboxylation leading to 5,6-dihydroxyindole (DHI or HQ) and 5,6-dihydroxyindole-2-carboxylic acid (DHICA) with final polymerization to melanin.<sup>2</sup> Currently, there is no general agreement on the secondary structure model because of the indetermination on the population of oxidized forms like indolequinone (IQ), quinone imine (QI), and semichinone (SQ), increasing the number of possible resulting configurations.

Such a large degree of freedom is reflected in two different popular structural models, namely, the heteropolymeric and oligomeric models: (a) Heteropolymeric melanin is formed by means of random bonds between monomers. This model is able to explain the optical and electric properties of the eumelanin, in

**Received:** April 11, 2011

**Revised:** August 12, 2011

**Published:** August 19, 2011

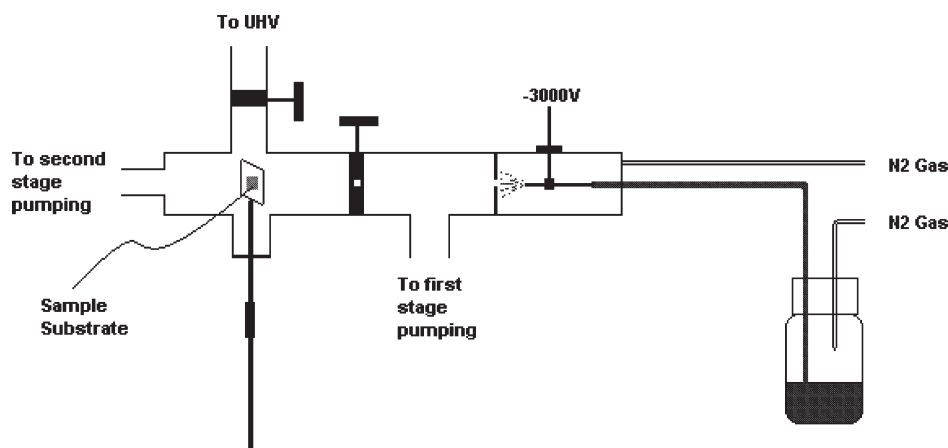


Figure 1. Electro spray system employed for the deposition of the ESD films.

particular, the wide absorption band, the chemical stability, and the little solubility.<sup>19</sup> (b) Oligomeric melanin is made by three or four layers of a protomolecule with five to six DHI/DHICA monomers, 15–20 Å large and 10–15 Å high. This model is supported by the atomic force microscopy (AFM) images.<sup>20–22</sup>

Recently, high-resolution microscopy images gave support to the latter model in both synthetic and natural melanin, where similar onion-like nanoaggregates with  $\pi$ – $\pi$  aromatic interaction and stacking distances of about 3.7 to 4.0 Å were observed.<sup>23</sup>

Our contribution to alleviate the problem of the reduced solubility, eventually improving the film growth quality, was through the use of the electro spray deposition (ESD) technique. Electro spray is commonly used in mass spectrometry, where the macromolecules are efficiently separated from the solvent through electroionization and also to prepare thin films under controlled ambient conditions<sup>24</sup> like in vacuum deposition on atomically clean substrates.<sup>25,26</sup> In this way, a controlled assembly and aggregation can be achieved. Two-dimensional growth of such biopolymer films will be obtained as the results of the isolation of the solute from the solvent and its direct interaction with the substrate, the film, or both; such an interaction is based on the “soft landing” on the surface and on the reduced effects of the ambient contaminants. Furthermore, for some applications like multicomponent films, multilayer films, or both, the present ESD technique might be very versatile.

In this work, we studied morphological, structural, electrical, and optical properties of the eumelanin films grown by ESD deposition. By changing the growth conditions, we observed modifications of the film characteristics, which only under specific extreme conditions could be addressed to a denaturation of the biopolymer but that can rather be put in relation with different monomers organization.

In the following, after a brief experimental description in Section II, we discussed the morphological, spectroscopic, and electrical properties in Section III. Scanning electron microscopy (SEM) and AFM were used to examine the morphological quality of the films. We carried out optical and X-ray photoelectron spectroscopy (XPS) to investigate the chemical composition and bonding character of the melanin, aiming at clarifying the molecular building blocks by Raman and Fourier transformed infrared (FTIR) spectroscopies and the electrical behavior through temperature-dependent I–V measurements. Conclusions will follow in Section IV.

## II. EXPERIMENTAL SECTION

Synthetic eumelanin powder was purchased from Sigma Aldrich and dissolved in dimethyl sulfoxide methanol solution (DMSO/CH<sub>3</sub>OH 1:20) in a concentration of 0.2 mg/mL. Figure 1 shows the ESD system used to prepare the melanin film on different substrates (indium–tin oxide (ITO), glass, SiO<sub>2</sub>, and ZnSe). A stainless-steel tip (inner diameter 0.1 mm) was modified through electrochemical etching in the H<sub>2</sub>SO<sub>4</sub>/H<sub>2</sub>O 1:1 solution to obtain a cone-shaped spray tip. A negative bias voltage was applied to the tip. When finely tuned, N<sub>2</sub> gas overpressurized the solution container, a controlled flow of solution could reach the spray tip, and electroionization occurred (so-called Taylor cone). Extracted from the grounded skimmer, the molecules were driven to the substrate using a differentially pumped system (the first stage at 1 Torr and the second stage at 10<sup>−3</sup> Torr).

ESD melanin films (300 nm thick) will be compared with spray-deposited (SD) films of comparable thickness.<sup>14</sup> In this latter case, the solution flux at the evaporator orifice was assisted by an out-flowing N<sub>2</sub> breath at a pressure of 0.6 mBar, and the substrate held at ~100 °C.

The morphology of the melanin film was monitored by SEM (Cambridge Stereoscan 360) and AFM (Veeco 5000 Dimension) working in noncontact mode with a cantilever frequency of 270 kHz. AFM quantitative morphological analysis was performed using WSxM software.<sup>27</sup>

Photoelectron spectroscopy measurements were performed using an Al K $\alpha$  unmonochromatized source (1486.7 eV) at a base pressure of 10<sup>−9</sup> Torr. The photoelectrons were analyzed with a cylindrical hemispherical analyzer (CHA) operating at a pass energy of 58 eV.

Investigation of the valence band spectra by means of ultraviolet photoelectron spectroscopy (UPS) was performed on samples grown on the ITO substrates to minimize charging effects. UPS spectra were acquired at pressure of ~10<sup>−9</sup> Torr using a He discharge lamp providing He I (21.2 eV) and He II (40.8 eV) lines impinging at 45° with respect to the detection direction of a VG-CLAM4 analyzer.

Absorption measurements were carried out by measuring the transmitted light intensity using Silicon PIN detector (Thorlabs DET110) and InGaAs PIN detector (Thorlabs DET10C). The signal was obtained by lock-in amplifier (EG&G model 5210) using optical chopper with the frequency of 30 Hz. MonoSpec

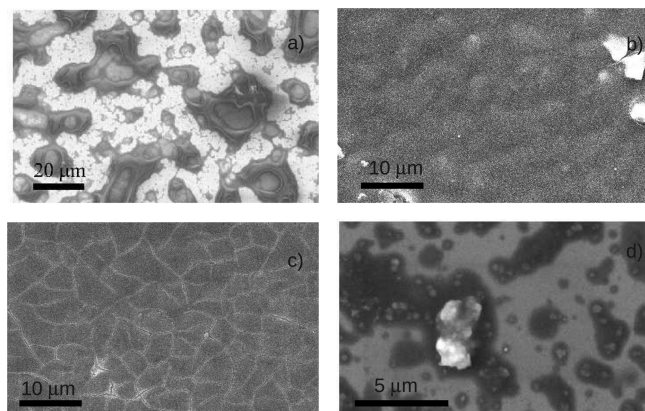


**Figure 2.** SEM images of spray-deposited film (a), electro spray deposited at a flow rate of  $1.3 \mu\text{L/s}$  and  $2 \text{ kV}$  (b), electro spray deposited at a flow rate of  $1.3 \mu\text{L/s}$  and  $3 \text{ kV}$  (c), and electro spray deposited at a flow rate of  $0.7 \mu\text{L/s}$  and  $3 \text{ kV}$  (d).

18 (Thermo Jarrel Ash), integrated with collimating mirror, grating (1200 grooves/mm for visible range and 600 grooves/mm for near-infrared region), and focusing mirror, served as the monochromator of the crystal halogen light source with the power of 100 W. Width of the entrance and exit slit were 500 and  $50 \mu\text{m}$ , respectively. Another exit focusing lens was used to increase the incoming light power on the sample. Absorption from both the substrate and the sample on the substrate was measured and normalized to take into account the energy dependence of the light source and optical parts.

FTIR analysis was performed using a Bruker Hyperion 3000 microscope coupled to a Bruker Equinox 55 interferometer modified to work in high vacuum; a conventional Globar source was used. A mercury–cadmium–telluride single pixel detector cooled to liquid nitrogen temperature and a KBr beam splitter were used. The experiments were performed in transmission configuration with a  $36\times$  objective and condenser using a double-sided, forward–backward acquisition mode of the interferometer. The IR spectra were taken in the wavelength range of  $650\text{--}4000 \text{ cm}^{-1}$  with a spectral resolution of  $4 \text{ cm}^{-1}$ . The microscope slits were closed at  $30 \times 30 \mu\text{m}^2$  to select a small area of the sample on the ZnSe substrate. A background spectrum was recorded as the average of several hundred scans in purged  $\text{N}_2$  atmosphere.

Raman measurements were taken by using a He–Ne ( $\lambda = 632.8 \text{ nm}$ ) laser source and spectrometer LabRam Infinity (Jobin-Yvon Horiba). A notch filter for the elastic contribution and holographic gratings with sinusoidal modulation with 1800 and 600 lines/mm respectively were used. The detector was Peltier-cooled, and several magnifications were available. A  $50\times$  objective allowed the visual inspection of the samples and the determination of the localized portion of the sample giving rise to the Raman spectrum. All spectra were taken by using a confocal diaphragm ( $100 \mu\text{m}$ ) to limit the beam dispersion. The power was taken between 0.15 and 15 mW to avoid sample degradation during the typical measurement time (between 100 and 150 s). The spectral resolution is 2 to  $3 \text{ cm}^{-1}$  for the holographic gratings with sinusoidal modulation with 1800 lines/mm.

Finally, the electric characterization was carried out under dark and controlled temperature conditions by a Keithley 617 electrometer in the V/I mode with gold stripes evaporated onto 7059 Corning glass substrates after film deposition.

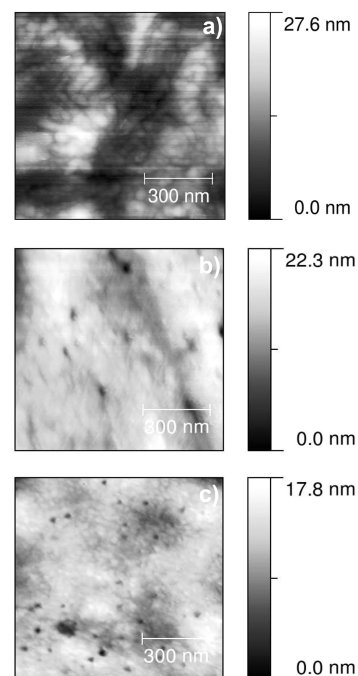


**Figure 3.** AFM topographs: (a) SD melanin, (b) ESD melanin film grown at  $2 \text{ kV}$  (rate  $1.3 \mu\text{L/s}$ ), and (c) ESD melanin film grown at  $3 \text{ kV}$  (rate  $1.3 \mu\text{L/s}$ ).

### III. RESULTS AND DISCUSSION

**A. Film Morphology.** Recent investigations on synthetic and natural melanins<sup>23</sup> provided evidence that the strikingly different morphology<sup>17,21</sup> observed on length scales of 100–200 nm was nearly vanishing when looking on a scale of a few nanometers. From our side, this work represented a contribution to increase further the thin films quality in terms of flatness and uniformity by deposition of synthetic melanin from organic solvents<sup>22</sup> through an advanced method. The difficulty to obtain high-quality smooth films suggested us to search for alternative routes like the SD technique by a  $\text{N}_2$  breathe<sup>14</sup> improving greatly the overall morphology. In this work, we showed that a further step can be obtained by ESD, leading to relatively thick and homogeneous films when compared with those grown by the SD technique.

In Figure 2a–d, SEM images of samples with comparable thicknesses (300 nm) grown, respectively, by SD and ESD were reported. SD melanin film, reported in Figure 2a, was discontinuous with several agglomerated islands, where the empty spaces were formed after solvent evaporation. It could also be observed that each block had flat and rather uniform terraces at the center and dunes at the side of the blocks, which were again due to the evaporation of the solvent. Further deposition filled up the spaces gradually, as could be seen in the thicker samples, however, it did not provide a continuous path for uniformity. In the case of ESD (Figure 2b) grown at  $2 \text{ kV}$ , the film exhibited rather different morphology. A lower amount of bare substrate was left, and the whole film was grown with uniform thickness, showing only slightly the globular characteristic corrugation of melanin films. As the voltage was increased from 2 to  $3 \text{ kV}$  (from b to c), the film became very flat with the formation of separation boundaries between the flat zones, probably due to strain; finally, if in addition the electro spray rate was lowered (from  $1.3 \text{ (c)}$  to  $0.7 \mu\text{L/s}$  (d)), then images suggested that a different 2D growth was occurring.

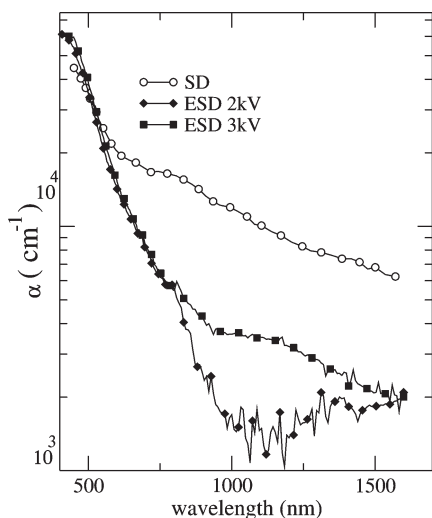


**Figure 4.** Optical absorption spectra of the SD and ESD melanin films at 2 and 3 kV voltage and a flow rate of  $1.3 \mu\text{L/s}$ .

From the AFM analysis in Figure 3a, the morphology of melanin obtained by SD with self-organization of globular structures of size 20–30 nm into larger structure of 100–200 nm size, leaving the surface highly corrugated, was reported. The ESD samples obtained at the flow rate of  $1.3 \mu\text{L/s}$  and at 2 and 3 kV, respectively, were reported in Figure 3b,c.

These images well resembled AFM images of device-quality melanin thin films obtained by Bothma and coworkers<sup>9</sup> by ammonia/water melanin solution, with the exception of a certain level of high-frequency roughness that is typical of the ESD technique.

In this case, the morphology showed less overall corrugation and flat elongated platelet were visible in the case of Figure 3b) (2 kV) (resembling a more oligomeric structure), eventually turning into smaller spherical particles 30–50 nm in the case of 3 kV deposition (Figure 3c)) but not showing any aggregation in larger structures. In this latter case, a cross-linking aggregation was probably developing, induced by hydrogenation of the structure.

**B. Optical Absorption.** Although absorption spectra resulted in being insensitive<sup>28</sup> to classify eumelanin types, for the sake of comparison with previous studies, we reported the absorption characteristics of thin films of synthetic melanins grown by both SD and ESD methods.

By looking at Figure 4, the spectra were characterized by smooth, structureless, wide band behavior, with exponential absorption at lower wavelengths<sup>13,29–31</sup> and optical density with steep increase in the visible range but without a clear-cut absorption edge. The exponential coefficient in the decay behavior was  $(7 \text{ and } 6) \times 10^{-3} \text{ nm}^{-1}$  for ESD and SD melanin, respectively, to be compared with values in literature around  $5 \times 10^{-3} \text{ nm}^{-1}$ .<sup>9</sup> Within samples grown by ESD, slight deviations occurred only in the near-infrared range. Mie scattering could play some role by tuning the tail part of the spectra at such a longer wavelength, where discrepancies are observed between the different samples<sup>32</sup> because of the agglomeration of monomers.

The results of the extrapolated onset of the absorption were between 1.2 and 1.55 eV for the ESD samples. These values were comparable to values ranging between 1.0 and 1.4 eV in the literature,<sup>13,33–35</sup> whereas a photopyroelectric determination of 1.7 eV was reported by de Albuquerque et al.<sup>36</sup>

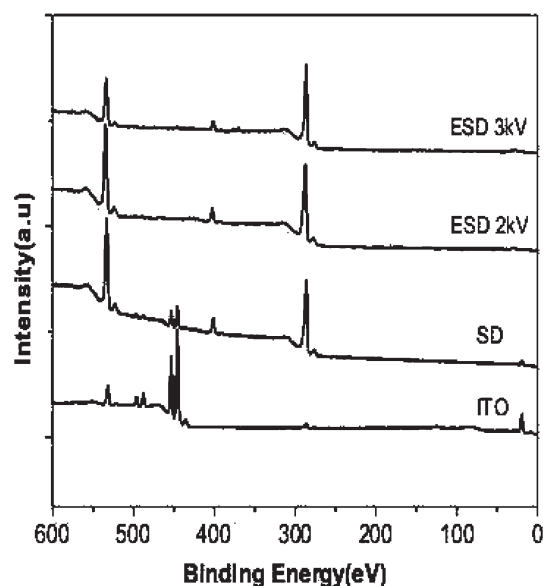


**Figure 5.** From bottom to the top are the XPS curves by Al  $K\alpha$  of ITO substrate, SD, and ESD melanin at 2 and 3 kV, respectively, with a flow rate of  $1.3 \mu\text{L/s}$ .

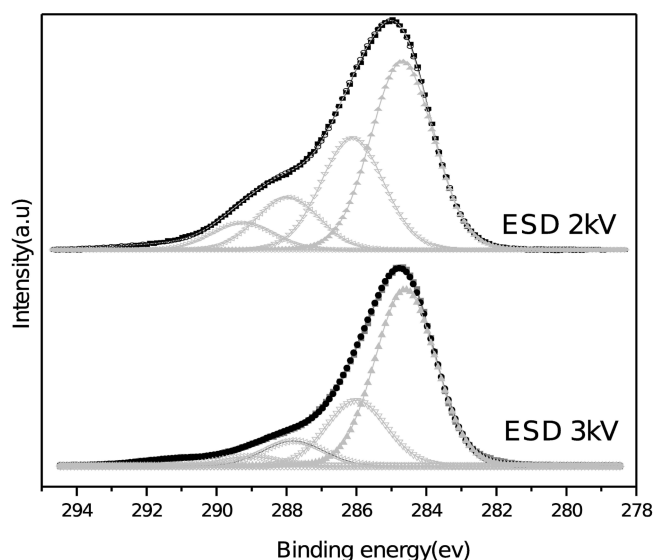


**Figure 6.** Photoemission spectra taken by Al  $K\alpha$  X-ray line. Decomposition of the C1s peak of the melanin film grown on ITO substrate by the ESD taken at 3 (lower curve) and at 2 kV (upper curve), both with a  $1.3 \mu\text{L/s}$  flow rate.

**C. Photoelectron Spectroscopy.** A first look to C1s (285 eV), N1s (400 eV), and O1s (530 eV) core levels in XPS of the melanin films reported in Figure 5 showed a good agreement between the SD and the ESD film grown at 2 kV (C1s/N1s ratio was  $\sim 5$ , whereas C1s/O1s ratio was  $\sim 1$ ). Such a N content was reduced by 50% when increasing the voltage from 2 to 3 kV, whereas the oxygen was reduced by 30%. As can be seen from Figure 5, there were no observable sulfur traces from the DMSO solvent, indicating a pure solute character of the films. The substrate resulted completely covered by the ESD films, whereas in the SD case some portions of the substrate were still visible by XPS as expected on the basis of the previous SEM analysis.

**Table 1. C1s Core Level Photoemission Chemical Shifted Components and Normalized Intensities for the ESD Melanin Films Grown on ITO at 2 and 3 kV and Rate of 1.3  $\mu\text{L/s}$**

C1s	BE shift (eV)	ESD-2 kV (norm. int.)	ESD-3 kV (norm. int.)
C–C	+0.0	4.0	5.3
C–N C–O	+1.3	2.7	2.0
C=O	+3.0	1.3	0.7
COOH	+4.7	0.6	0.3
$\pi-\pi^*$	+6.5	0.2	0.3

To determine the details of the chemical configuration, we took a closer look at the C1s core level. (See Figure 6.) To this aim, the C1s core level was decomposed into five chemically shifted components with characteristic binding energy shift values<sup>37–39</sup> with respect to the C–C and C–H bonds at 285.0 eV; C–O, C–N, and C=N bonds shifted by 1.3 eV; carbonyl (C=O) at 3.0 eV; carboxyl group (COOH) at 4.7 eV; and the peak due to  $\pi-\pi^*$  shakeup satellite at the energy of 6.5 eV higher binding energy.

In Table 1, we reported the result of the fit of the binding energy values and of the normalized areas of the components of spectra reported in Figure 6 for the two ESD samples grown, respectively, at 2 and 3 kV.

By comparing the peak areas, after the subtraction of the background and the  $\pi-\pi$  satellite component, it was possible to establish the chemical composition of the monomers.

To this aim, in addition to the carboxyl carbon when present, a proper normalization of the total area of the C1s core level peak was due to a total number of eight C atoms, respectively, for the two C–N, four C–C, and two C=(–)O<sup>14</sup> bonds.

From both the stoichiometric ratio and the analysis of the nitrogen 1s core level, showing the presence of a single component at 400 eV BE like in pyrrole molecules, we found indications that the structure of the monomers was preserved, as shown by the work of Malitesta et al.<sup>40</sup> From the elaboration of the data, it was possible to determine that the number of carboxyl groups per monomer was  $\sim 0.60$ , indicating an equivalent 60% probability of DHICA-type monomers occurring. Such a carboxylic component was statistically larger than that found in the case of the SD melanin<sup>14</sup> (0.46), proving a different character for the two deposited films, with the higher value of carboxyl groups being more compatible with an oligomeric structure.

In the case of ESD films grown at higher voltage (3 kV), a progressive reduction of the C–N and C–O components was observed (Table 1) with the COOH amounting to about one half of the initial value. An equivalent increase in the contribution from aliphatic groups was expected from the saturation of broken bonds. The reduced number of carboxyl groups and C–N bonds is then responsible for the progressive cross-linking bonding of monomers.

Such a situation was the result of a combined effect due to electric field intensity and to the longer exposure time to such a field.

For instance, in the case of a flow rate of  $\sim 0.7 \mu\text{L/s}$  for the optimal solution concentration of 0.1 to 0.2 mg/mL, C1s spectra (not reported) showed only a minor C1s component from C–N and C–O bonds at 286.3 eV,  $\sim 15\%$  of the intensity of the main C1s peak at 285 eV. In this case, the opening of the pyrrole ring of the eumelanin monomer could be at the origin of such a spectrum.

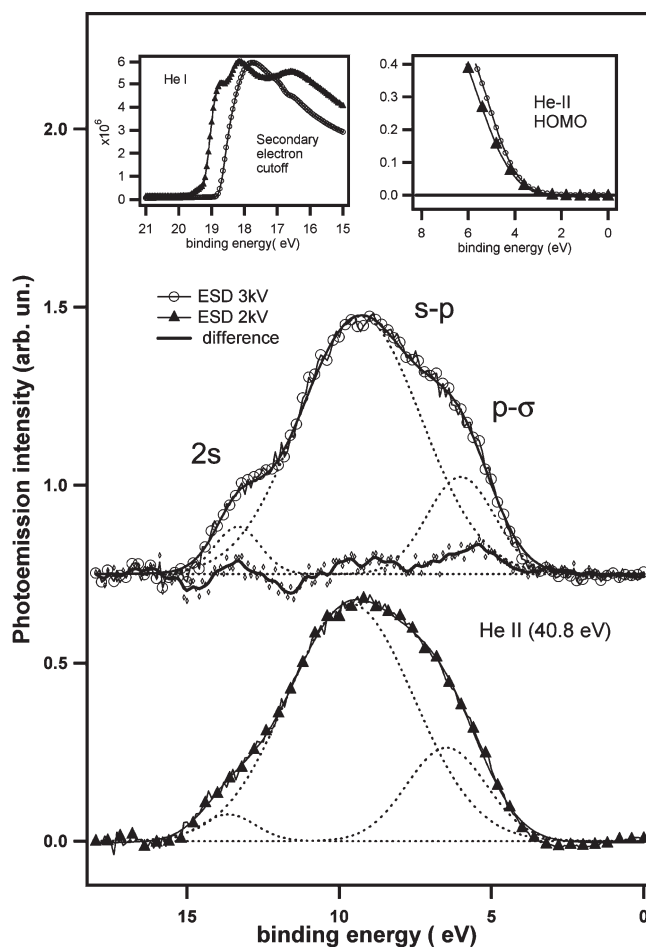


**Figure 7.** Ultraviolet photoemission spectroscopy of the ESD melanin films grown on ITO substrates (respectively, with 2 and 3 kV) obtained with He II source (40.8 eV). The change from the 2 to the 3 kV ESD film was reported in the difference curve. The right inset shows the region of the Fermi energy, whereas on the left inset the secondary electron edge is observed by the He I source (21.2 eV) and a bias of  $-10$  V.

We presented in Figure 7 the ultraviolet photoemission spectroscopy (UPS) of the melanin films grown on top of a ITO substrate obtained with He II source (40.8 eV), showing a typical intense emission around 10 eV due to a mixture of localized p and delocalized s states. A shoulder at 6 eV BE due to p and  $\sigma$  states<sup>35</sup> is also evident. Finally, 2s states are present close to 13 eV BE. Basically, we observed a shift to lower binding energies of the p– $\sigma$  and s–p states consistent with a sizable reduction of the N content in the structure.<sup>41</sup> A marked  $\sigma$  character (as shown by the difference curve) when the voltage is increased could indicate a stronger cross-linking between different monomers and lack of conjugation by  $\pi$  orbitals.

The first ionization potential (IP) of the films was determined by the difference between the photon energy and the spectrum width from secondary electron cutoff to HOMO level (2 eV BE for melanin film, in agreement with a report by Sangaletti et al.<sup>35</sup>). We applied 10 V of negative bias voltage to the sample to pinpoint the secondary electron cutoff. By the way, a similar determination in the case of the SD films was difficult because of the noncontinuous coverage of the ITO substrate. In the case of the electrospray under 2 kV voltage, a value of IP of 4.6 eV was found, whereas in the case of a higher voltage applied (3 kV), a

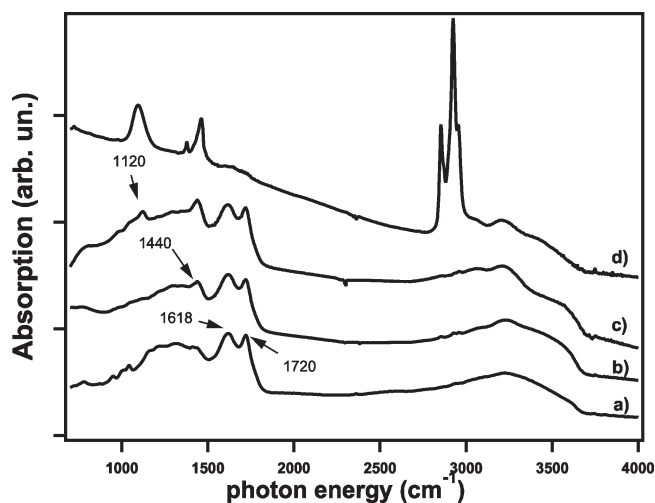


**Figure 8.** IR absorption spectra of melanin thin films grown on ZnSe substrates. From the bottom to the top were reported: (a) SD melanin, (b) ESD at 2 kV, (c) ESD at 3 kV, and (d) ESD at 3 kV and  $0.7 \mu\text{L/s}$ .

reduction of the IP to  $\sim 4$  eV was observed due to the reduced amount of oxygen and the increase in hydrogenation in the structure.

**D. Infrared Spectroscopy.** We have performed IR absorption experiments on melanin grown on ZnSe substrates to investigate the melanin structure on a more extended spatial range with respect to short-range probed by photoelectron spectroscopies. The IR absorption spectra of melanin films are reported in Figure 8: (a) film grown by SD; (b) ESD film grown at a flow rate of  $1.3 \mu\text{L/s}$  by a voltage of 2 kV; (c) same growth rate but at 3 kV; and (d) film grown at 3 kV and at flow rate of  $0.7 \mu\text{L/s}$ .

Both the SD (Figure 8a) and ESD (Figure 8b,c) spectra, with the exception of the spectrum reported in Figure 8d, are characterized by large absorption in the region at  $1464 \text{ cm}^{-1}$  due to C–N and  $\sim 1535 \text{ cm}^{-1}$  due to pyrrole breathing, whereas the COOH stretching is close to  $1720 \text{ cm}^{-1}$ .<sup>42,43</sup> All of these features indicated a strong DHICA content in these films. Furthermore, the SD film showed the largest intensity in the  $1200\text{--}1320 \text{ cm}^{-1}$  region due to the bending of –OH groups in DHI monomers.

The spectrum reported in Figure 8d was the result of the combination of high voltage (3 kV) and low flow rate ( $0.7 \mu\text{L/s}$ ) and developed a strong absorption occurring at 2854 and  $2923 \text{ cm}^{-1}$  that can be assigned to the stretching vibration of the aliphatic groups<sup>44,45</sup> and in general to hydrogen terminations.

From all of these effects, an important role played by the DHICA monomers in the SD and ESD melanin (Figure 8b,c) in the move from an extended heteropolymeric aggregation to fragmentation and stacking of planar oligomers composed of a few monomers was derived.

IR data confirmed that when the biopolymer is exposed for a long time to high electric field, as in the case of film obtained by using a voltage of 3 kV and a low rate of  $0.7 \mu\text{L/s}$ , and in general the growth is slowed by the poor efficiency of the spray system, a different structure was observed. Such a configuration is distinctively different from that of the graphitic amorphous carbon<sup>46</sup> and was in fact showing cross-linking quality signatures in the region between  $1000$  and  $1600 \text{ cm}^{-1}$ .<sup>1,47</sup>

**E. Raman Spectroscopy.** The results obtained by the analysis of the IR spectra were consistent with what was observed from Raman spectroscopy.

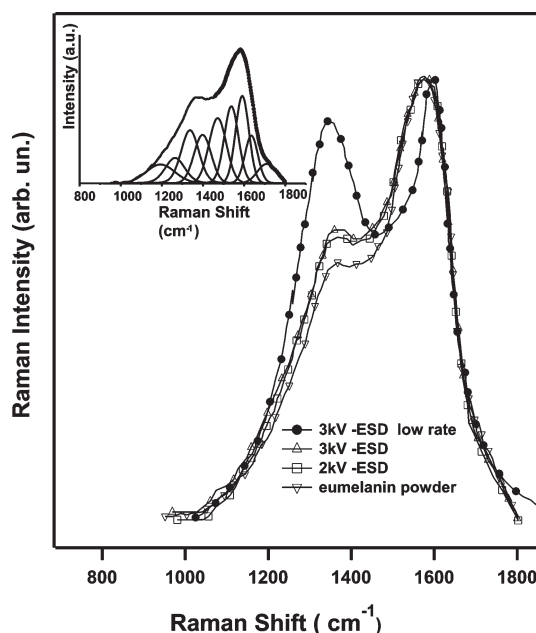


**Figure 9.** Raman spectra of SD and ESD at different voltages and flow rates (2 and 3 kV at  $1.3 \mu\text{L/s}$  and 3 kV at  $0.7 \mu\text{L/s}$ ) on ZnSe substrates. In the inset is reported the fitting plot of the experimental Raman of ESD 2 kV sample and the nine components at frequencies reported in Table 2.

ESD films investigated appeared to be rather homogeneous either by visual inspection with microscope or by the Raman spectroscopic analysis, allowing a spatial resolution on the sample surface of  $<1 \mu\text{m}$ . Raman spectra were collected from different samples prepared by as-purchased eumelanin powder or ESD under different conditions. For SD films, although not completely homogeneous, the spectra were taken by averaging on different points on the samples, and the resulting spectrum was comparable to the result obtained from the as-purchased powder.

A fluorescence background contribution<sup>34,48,49</sup> has been subtracted from all of the spectra collected. This procedure did not affect the analysis of the Raman response, giving the same results using quite different subtraction strategies.

Using a standard procedure, the Raman spectra were analyzed by means of a linear combination of damped harmonic oscillators.<sup>50</sup>

The Raman signals were fitted using the Levenberg–Marquardt algorithm<sup>51,52</sup> with nine components over the  $950\text{--}1800 \text{ cm}^{-1}$  range. The number of components and the frequencies of each component were determined through a second-derivative analysis. The best-fitting curve is shown in the inset of Figure 9 together with the respective nine components.

The best-fit values of the component frequencies in the case of as purchased powder are reported in Table 2 together with standard deviations. Almost no deviations from this values are observed when analyzing other considered samples.

It is important to take into consideration the fact that the comparison with the experimental quantities was based on data taken from gas and liquid phases to be extrapolated to present thin film data.

Spectra collected from the four samples are shown in Figure 9.

From the analysis of Figure 9, the increase in the voltage during ESD preparation enhanced the Raman intensity in the region of  $1300 \text{ cm}^{-1}$  and determined a reduction in the range of  $1600 \text{ cm}^{-1}$ . The former effect was due to the increase in C–H

deformation, whereas the latter effect was due to the reduction of N and O contribution (indole and pyrrole ring vibration).

It is worth noting that typical Raman spectra of the melanin resembled that of amorphous carbon graphitic structure with an important G band at  $1600\text{ cm}^{-1}$ , whereas the material more exposed to the electric field was successfully compared with

**Table 2. Raman Shift Frequencies and Assignments (s = stretching, d = deformation) for Eumelanin As-Purchased Powder**

assignment	Raman shift ( $\text{cm}^{-1}$ )
s(C–C) ring breathing	$1191 \pm 2$
d(C–H) in plane	$1261 \pm 2$
indole ring vibration/s (CN)	$1336 \pm 2$
s(pyrrole ring)	$1398 \pm 2$
C=C aromatic ring vibration/s sym(COO <sup>−</sup> )	$1470 \pm 2$
C=C aromatic/pyrrole ring stretching vibration	$1539 \pm 2$
s(C=C aromatic)/s(pyrrole ring)/indole ring vibration	$1593 \pm 2$
C=C aromatic ring vibration/s antisymmetric (COO <sup>−</sup> )	$1637 \pm 2$
s(C=O in COO <sup>−</sup> , quinone, or ketone)	$1706 \pm 2$

hydrogenated nanocrystalline diamond with strong D band at  $1300\text{ cm}^{-1}$  and a narrow peak at  $1600\text{ cm}^{-1}$ .<sup>46</sup>

**F. Transport.** The transport properties of synthetic melanin films were measured in the dark and in nitrogen-gas-saturated atmosphere to avoid any effect from the surroundings, as previously mentioned by Goncalves et al.<sup>53</sup> for melanin samples in the form of pellets. In Figure 10, the electrical properties at different temperatures of a 100 nm thick film of melanin grown on glass at a voltage of 3 kV and flow rate of  $1.3\text{ }\mu\text{L/s}$  are reported. The structure was planar with a gap of  $50\text{ }\mu\text{m}$  between two 100 nm Au deposited electrodes. The resistance (panel a) as a function of the temperature for the melanin thin film decreased by four orders of magnitude from room temperature (RT) to 480 K, which suggested the semiconductor-like behavior.<sup>14</sup>

The lower resistance for ESD melanin thin film confirmed the advances in morphology and continuity and intermonomer transport of ESD films as compared with SD melanin thin films.<sup>14</sup> No hysteresis after heating–cooling T runs was observed as previously found for SD films, which was ascribed to the easy water removal from the molecule. This might be due to the much drier nature of ESD films.

Two activation energies were found at 0.76 and 1.26 eV for the lower and higher temperature parts of the spectrum, with the

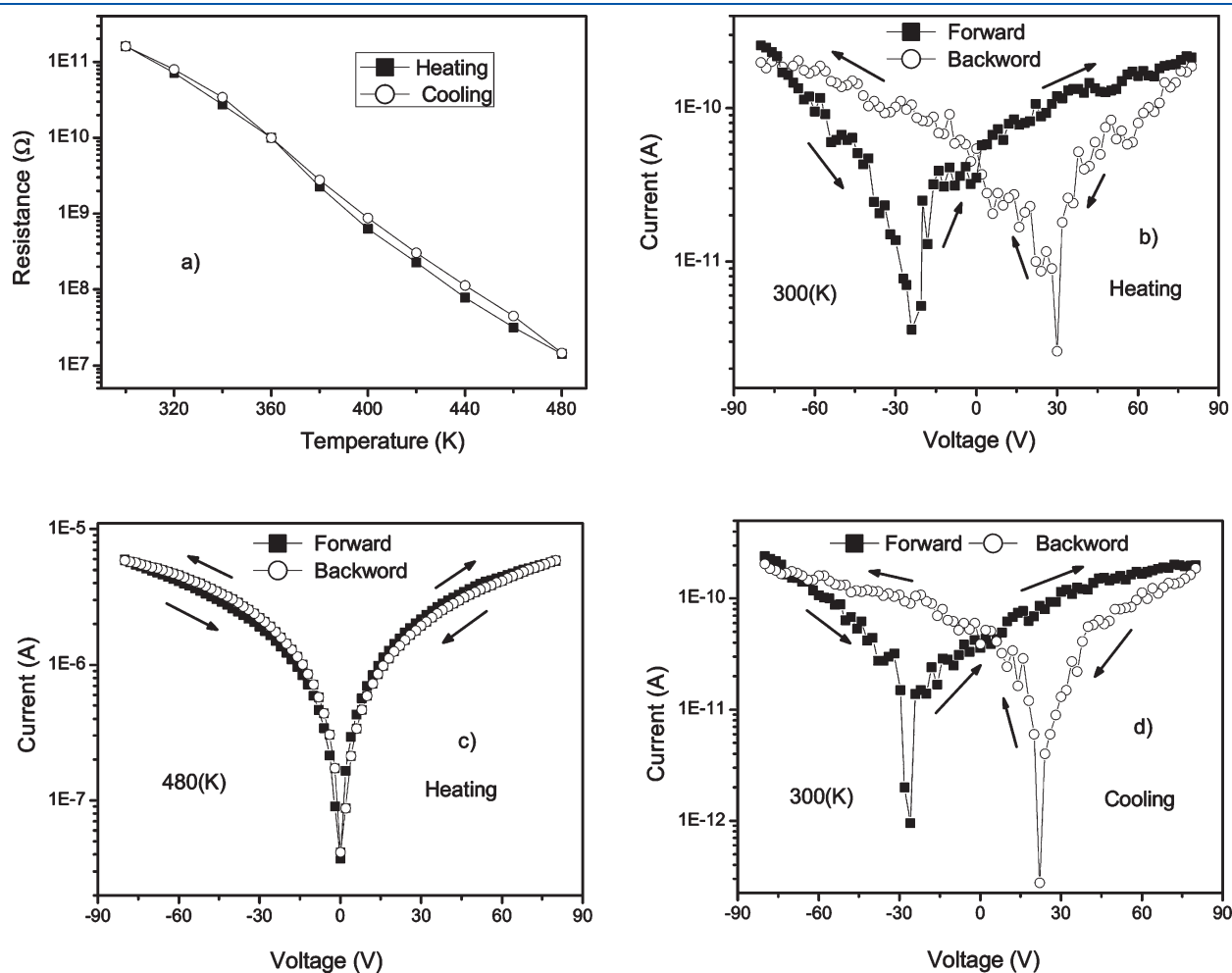


**Figure 10.** Electrical properties of ESD synthetic eumelanin thin films at different temperatures in the dark under nitrogen conditions of a planar melanin structure between two Au electrodes separated by  $50\text{ }\mu\text{m}$ . (a) Resistance as a function of the temperature for the thin film during heating and cooling. (b–d) Measured in both forward and backward voltage sweep directions at different temperatures during heating and cooling processes.

former one being consistent with that found in the SD films.<sup>14</sup> In the lower temperature range, below 370 K, the lower activation energy could be related to bound water, to positive carriers,<sup>53</sup> or both, with the occurrence of charge buildup at the electrodes because of inefficient charge transfer. Above such a temperature, the thermal load distortion induced in the structure is able to provide enough electrons to give rise to an apparent ohmic behavior with no hysteretic or buildup effects.

I–V characteristic of a melanin thin film were measured in both forward and backward voltage sweep directions at different temperatures. Interesting results were observed during heating and cooling processes. At RT, hysteretic behavior was found; as the temperature of the samples was increased, the hysteretic behavior diminished continuously, as reported in Figure 10 from b to d. Such a characteristic could rise from the presence of shallow trap states in melanin film. At RT, the injected charges were trapped, and compensation of local field occurred because of the screening effect. During temperature increase, the trapped charges were released immediately with the help of phonon-assisted hopping.

#### IV. DISCUSSION AND CONCLUSIONS

The aim of the present work was to characterize largely planar and homogeneous eumelanin homogeneous thin films on a scale of several millimeters. The control of specific parameters during the growth process allows some rationalization on the functionalization of this important biopolymer. To do this, the solvent/substrate interaction during the film formation was limited, inducing a sizable control in the film self-aggregation.

SEM and AFM analysis evidenced that by using the ESD technique one can obtain uniform and rather flat melanin films with controllable thickness, ensuring the full coverage of the substrate.

It was verified by XPS that the contribution of 60% carboxylic-acid-related subunit to the oligomeric secondary structure of the molecule was larger than the value measured in SD films (45%). Such a carboxylic contribution could trigger the secondary structure of the melanin aggregates, reducing the number of random bonding between monomers, enhancing in this way the oligomeric aggregation with respect to a heteropolymeric conformation of the biomaterial.

Another aspect is the integrity of the aromaticity of the pyrrole ring related to a more graphitic electronic structure measured by UPS, which changed during the electric field variation. Similar effects are observed by IR and Raman data, putting into evidence again the transition from a more graphitic structure to a novel biomaterial with a more 3D character, similar to that of hydrogenated nanocrystalline diamonds, with dominant cross-linking. Finally, I–V characteristics showed a drier nature of the present samples, a necessary prerequisite to investigate the fundamental transport mechanism in this biomaterial. It is worth stressing that the ESD technique not only was proven to preserve the melanin characteristic structure but also was proven to enhance the oligomeric character with respect to the heteropolymeric random bonding in materials obtained by using other techniques, opening the way to a quite peculiar tailoring of the melanin. Further improvement could be reached by combining the present tool with more specific solvent choices or thermal procedures to improve the level of the film quality and of the characterization.

#### AUTHOR INFORMATION

##### Corresponding Author

\*E-mail: roberto.gunnella@unicam.it.

#### ACKNOWLEDGMENT

Dr. L. Petetta is acknowledged for assistance during SEM measurements at the CGA center of University of Camerino.

#### REFERENCES

- (1) Prota, G. *J. Invest. Dermatol.* **1980**, *75*, 122.
- (2) Felix, C. C.; Hyde, J. S.; Sarna, T.; Sealy, R. C. *J. Am. Chem. Soc.* **1978**, *100*, 3922.
- (3) Nicolaus, R. A.; Piattelli, M.; Fattorusso, E. *Tetrahedron* **1964**, *20*, 1163.
- (4) Albanese, G.; Bridelli, M. G.; Deriu, A. *Biopolymers* **1984**, *23*, 1481.
- (5) Berggren, M.; Richter-Dahlfors, A. *Adv. Mater.* **2007**, *19*, 3201.
- (6) Ambrico, M.; Cardone, A.; Ligonzo, T.; Augelli, V.; Ambrico, P.; Cicco, S.; Farinola, G. M.; Filannino, M.; Perna, G.; Capozzi, V. *Org. Electron.* **2010**, *11*, 1809.
- (7) Lee, H.; Rho, J.; Messersmith, P. B. *Adv. Mater.* **2009**, *21*, 431.
- (8) Bettinger, C. J.; Bruggeman, P. P.; Misra, A.; Borenstein, J. T.; Langer, R. *Biomaterials* **2009**, *30*, 3050.
- (9) Bothma, J. P.; de Boor, J.; Divakar, U.; Schwenn, P. E.; Meredith, P. *Adv. Mater.* **2008**, *20*, 3539.
- (10) d'Ischia, M.; Napolitano, A.; Pezzella, A.; Meredith, P.; Sarna, T. *Angew. Chem., Int. Ed.* **2009**, *48*, 3914.
- (11) McGinness, J. E. *Science* **1972**, *177*, 896.
- (12) McGinness, J. E.; Corry, P.; Proctor, P. *Science* **1974**, *183*, 853.
- (13) Crippa, R. P.; Cristoforetti, V.; Romeo, N. *Biochim. Biophys. Acta* **1978**, *538*, 164.
- (14) Abbas, M.; D'Amico, F.; Morresi, L.; Pinto, N.; Ficcadenti, M.; Natali, R.; Ottaviano, L.; Passacantando, M.; Cuccioli, M.; Angeletti, M.; Gunnella, R. *Eur. Phys. J. E* **2009**, *28*, 285.
- (15) Seppa, H. *IEEE Trans. Appl. Supercond.* **2001**, *11*, 759.
- (16) Meredith, P.; Powell, B. J.; Riesz, J.; Nighswander-Rempel, S. P.; Pederson, M. R.; Moore, E. G. *Soft Matter* **2006**, *2*, 37 and references therein.
- (17) Liu, Y.; Simon, J. D. *Pigm. Cell Res.* **2003**, *16*, 606 and references therein.
- (18) Borghetti, P.; Goldoni, A.; Castellarin-Cudia, C.; Casalis, L.; Herberg, F.; Floreano, L.; Cossaro, A.; Verdini, A.; Gebauer, R.; Ghosh, P.; Sangaletti, L. *Langmuir* **2010**, *26*, 19007.
- (19) Pullman, A.; Pullman, B. *Biochim. Biophys. Acta* **1961**, *54*, 384.
- (20) Zajac, G. W.; Gallas, J. M.; Alvarado-Swaigood, A. E. *J. Vac. Sci. Technol., B* **1994**, *12*, 1512.
- (21) Clancy, C. M. R.; Simon, J. D. *Biochemistry* **2001**, *40*, 13353.
- (22) Lorite, G. S.; Coluci, V. R.; da Silva, M. I. N.; Deziderio, S. N.; Graeff, C. F. O.; Galvao, D. S.; Cotta, M. A. *J. Appl. Phys.* **2006**, *99*, 113511.
- (23) Watt, A. A. R.; Bothma, J. P.; Meredith, P. *Soft Matter* **2009**, *5*, 3754.
- (24) Jaworek, A. *J. Mater. Sci.* **2007**, *42*, 266.
- (25) Swarbrick, J. C.; Taylor, J. B.; O'Shea, J. N. *Appl. Surf. Sci.* **2006**, *252*, 5622.
- (26) Dam, N.; Beerbom, M. M.; Braunagel, J. C.; Schlafa, R. *J. Appl. Phys.* **2005**, *97*, 024909.
- (27) Horcas, I.; Fernandez, R.; Gomez-Rodriguez, J. M.; Colchero, J.; Gomez-Herrero, J.; Baro, A. M. *Rev. Sci. Instrum.* **2007**, *78*, 013705.
- (28) Meredith, P.; Sarna, T. *Pigm. Cell Res.* **2006**, *19*, 572.
- (29) Sarna, T.; Sealy, R. C. *Photochem. Photobiol.* **1984**, *39*, 69.
- (30) Kollias, N.; Baqer, A. H. *J. Invest. Dermatol.* **1987**, *89*, 384.
- (31) Nighswander-Rempel, S.; Riesz, J.; Gilmore, J.; Bothma, J.; Meredith, P. *J. Phys. Chem. B* **2005**, *109*, 20629.
- (32) Riesz, J.; Gilmore, J.; Meredith, P. *Biophys. J.* **2006**, *90*, 4137.

- (33) Ligonzo, T.; Ambrico, M.; Augelli, V.; Perna, G.; Schiavulli, L.; Tamma, M. A.; Biagi, P. F.; Minafra, A.; Capozzi, V. *J. Non-Cryst. Solids* **2009**, *355*, 1221.
- (34) Capozzi, V.; Perna, G.; Gallone, A.; Biagi, P. F.; Carmone, P.; Fratello, A.; Guida, G.; Zanna, P.; Cicero, R. *J. Mol. Struct.* **2005**, *744*, 717.
- (35) Sangaletti, L.; Pagliara, S.; Vilmercati, P.; Castellarin-Cudia, C.; Borghetti, P.; Galinetto, P.; Gebauer, R.; Goldoni, A. *J. Chem. Phys. B* **2007**, *111*, 5372.
- (36) de Albuquerque, J. E.; Giacomantonio, C.; White, A. G.; Meredith, P. *Eur. Biophys. J.* **2006**, *35*, 190.
- (37) Lebugle, A.; Subirade, M.; Gueguen, J. *Biochem. Biophys. Acta* **1995**, *1248*, 107.
- (38) Fontaine, L.; Lemele, T.; Brosse, J. C.; Sennyey, G.; Senet, J. P.; Wattiez, D. *Macromol. Chem. Phys.* **2002**, *203*, 1377.
- (39) Davidson, M. R.; Mitchell, S. A.; Bradley, R. H. *Surf. Sci.* **2005**, *581*, 169.
- (40) Malitesta, C.; Losito, I.; Sabbatini, L.; Zambobin, P. G. *J. Electron Spectrosc. Relat. Phenom.* **1995**, *76*, 629.
- (41) Bhattacharyya, S.; Spaeth, C.; Richter, F. *J. Appl. Phys.* **2001**, *89*, 2412.
- (42) Okuda, H.; Nakamura, A.; Wakamatsu, K.; Ito, S.; Sato, T. *Chem. Phys. Lett.* **2007**, *433*, 355.
- (43) Powell, B. J.; Baruah, T.; Bernstein, N.; Brake, K.; McKenzie, R. H.; Meredith, P.; Pederson, M. R. *J. Chem. Phys.* **2004**, *120*, 8608.
- (44) Harki, E.; Talou, T.; Dargent, R. *Food Chem.* **1997**, *58*, 69.
- (45) Bilinska, B. *Spectrochim. Acta, Part A* **2001**, *57*, 2525.
- (46) Nagano, A.; Yoshitake, T.; Hara, T.; Nagayama, K. *Diamond Relat. Mater.* **2008**, *17*, 1199.
- (47) Majumdar, A.; Scholz, G.; Hippler, R. *Surf. Coat. Technol.* **2009**, *203*, 2013.
- (48) Meredith, P.; Riesz, J. *J. Photochem. Photobiol.* **2004**, *79*, 211.
- (49) Perna, G.; Frassanito, M. C.; Palazzo, G.; Gallone, A.; Mallardi, A.; Biagi, P. F.; Capozzi, V. *J. Lumin.* **2009**, *129*, 44.
- (50) Postorino, P.; Congeduti, A.; Degiorgi, E.; Itie, J. P.; Munsch, P. *Phys. Rev. B* **2002**, *65*, 224102.
- (51) Marquardt, D. W. *J. Appl. Math.* **1963**, *11*, 431.
- (52) Levenberg, K. *Q. Appl. Math.* **1944**, *2*, 164.
- (53) Goncalves, P. J.; Baffa Filho, O.; Graeff, C. O. F. *J. Appl. Phys.* **2006**, *99*, 104701.